

Generating–absorbing sponge layers for phase-resolving wave models



Yao Zhang^a, Andrew B. Kennedy^{a,*}, Nishant Panda^b, Clint Dawson^b, Joannes J. Westerink^a

^a Department of Civil Engineering and Geological Sciences, University of Notre Dame, Notre Dame, IN 46556, USA

^b Department of Aerospace Engineering and Engineering Mechanics, The University of Texas at Austin, 210 East 24th Street, W.R. Woolrich Laboratories, 1 University Station, C0600, Austin, TX 78712-0235, USA

ARTICLE INFO

Article history:

Received 7 November 2012

Received in revised form 21 October 2013

Accepted 24 October 2013

Available online xxxx

Keywords:

Water waves

Boussinesq equations

Computational methods

ABSTRACT

The accurate generation and absorption of water waves in phase-resolving models are critical issues in representing nearshore processes. Here, we present a source function method for combined wave generation and absorption using modified sponge layers. This technique can be easily adapted to a wide variety of systems, and does not require the solution of Green's functions but rather the simpler knowledge of solutions for free waves. These solutions may be linear or nonlinear, regular or irregular, and generated waves can be made arbitrarily accurate through simple selection of sponge layer coefficients. Generating–absorbing sponge layer systems are shown to have a close correspondence to relaxation zones for wave generation if relaxation coefficients are chosen appropriately.

© 2013 Elsevier B.V. All rights reserved.

1. Introduction

The generation and absorption of waves at the boundary are important for the numerical simulation of Boussinesq and other water wave models. Relatively straightforward methods used by [Nwogu \(1993\)](#), [Kennedy and Fenton \(1997\)](#) and many others specified the incident wave information at the wavemaker boundary, with either no special treatment for reflected waves or approximate boundary conditions. These types of boundaries are compact and save on computational expense, but treatment for outgoing waves is by necessity approximate. Other techniques include various widely-used internal generation methods using either distributed or point sources in the governing equations ([Chawla and Kirby, 2000](#); [Larsen and Dancy, 1983](#); [Slotner and Apelt, 1999](#); [Wei and Kirby, 1999](#)). Relaxation zones ([Madsen et al., 2003](#)), where an imposed solution is gradually transitioned to the governing equations over some distance, have been used both to generate and absorb waves in high accuracy Boussinesq models.

Associated with the wave generation problem is that of absorbing reflected or other waves that approach open boundaries. Here, by far the most common techniques are the various sponge layers (e.g., [Chawla and Kirby, 2000](#); [Larsen and Dancy, 1983](#)) that extract mass, momentum, or both from the system, damping solutions to a steady-state with no waves. For nonlinear wave generation, both direct imposition of boundary fluxes and relaxation zones have been demonstrated to work, but accurate nonlinear wave generation using internal sources is quite difficult, and no good solutions exist.

This paper introduces and tests a combined generating–absorbing condition for phase-resolving wave models that is straightforward to

apply to a wide variety of systems. The condition does not require derivation of Green's functions as with many internal generators ([Chawla and Kirby, 2000](#)) but instead requires a knowledge of free wave solutions, which are simpler to derive and are known for a wide range of equations. These free wave solutions may be linear or nonlinear, regular or irregular, and may be reproduced to arbitrary levels of accuracy. At the same time as the system generates waves, it absorbs outgoing signals in the same way as a typical sponge layer. Analytical and numerical tests show excellent performance for a range of conditions including irregular, nonlinear, wave generation.

2. Generating–absorbing sponge layers

The concept of sponge layers was introduced by [Israeli and Orszag \(1981\)](#), and is widely used to remove unwanted signals at the edge of domains, and prevents them from re-reflecting off open boundaries. For the present paper, it may be extended and written as

$$[\mathbf{A}_1][\mathbf{a}_t] + [\mathbf{L}_1][\mathbf{a}_t] + \text{other terms} = \omega_1[\mathbf{A}_1][\mathbf{a}_{imp} - \mathbf{a}] + \omega_2[\mathbf{L}_1][\mathbf{a}_{imp} - \mathbf{a}] \quad (2.1)$$

where $[\mathbf{a}](x,y,t)$ is the vector of variables (which would be $(\eta, U, V)^T$ for many Boussinesq-type systems where η is the surface elevation and (U, V) are the velocity variables, $\mathbf{a}_{(-)} \equiv \partial \mathbf{a} / \partial (-)$, $\omega_1(x,y)$ and $\omega_2(x,y)$ are non-negative real damping coefficients. The matrix $[\mathbf{A}_1]$ contains algebraic multipliers of $[\mathbf{a}_t]$ (e.g., 1 or h) while the matrix $[\mathbf{L}_1]$ contains spatial differential operators of $[\mathbf{a}_t]$ (e.g., $h^2 \partial^2 / \partial x^2$). In other words, ω_1 may be thought of as modifying pure time derivative terms in the system, while ω_2 modifies mixed space–time terms. Together, they contain all time derivative terms that may be operated on by damping. Separate

* Corresponding author.

E-mail address: andrew.kennedy@nd.edu (A.B. Kennedy).

damping coefficients are used as it will be shown that there are advantages and disadvantages to using both forcings, depending on the situation.

The heart of the system is the vector of imposed quantities, $[\mathbf{a}_{imp}](x, y, z, t)$. For typical water wave implementations (Wei and Kirby, 1999) velocities would be damped towards zero, with perhaps elevation damping to a desired tide level, leading to a system which damps towards quiescence. However, damping to zero is not always necessary or even helpful. Here we specify that imposed quantities $[\mathbf{a}_{imp}](x, y, t)$ must be homogeneous solutions to the undamped system, i.e., Eq. (2.1) with $\omega_1 = \omega_2 = 0$. These imposed quantities are the desired waves to be generated, and may be linear or nonlinear, steady or unsteady.

By inspection, we see that if $[\mathbf{a}] = [\mathbf{a}_{imp}]$, the right hand side of Eq. (2.1) is zero and the desired free wave propagates identically to the undamped equations. However, if $[\mathbf{a}] \neq [\mathbf{a}_{imp}]$, the right hand side terms in Eq. (2.1) will gradually force the solution towards $[\mathbf{a}_{imp}]$ in the same way that a standard sponge layer forces velocities and/or elevations to zero. In this way, the system can generate the imposed waves at the same time as it damps other disturbances like reflected waves. Generation and absorbing zones are placed along the boundaries, and are the only locations where ω_1 and ω_2 are nonzero. If $[\mathbf{a}_{imp}] = 0$, the system becomes a normal sponge layer.

The utility of this combined generation/damping layer is easy to see. By not requiring two separate generation/absorbing layers as with Wei and Kirby (1999) or Chawla and Kirby (2000), space is saved. Undamped free waves are relatively easy to derive compared to the Green's functions in internal wavemakers, or may even be taken from other model outputs. Nonlinear waves, which are a significant issue for internal wave generators using Green's functions, are easy to generate with this new method as long as free wave solutions are known for the system variables. There are only two significant issues to be dealt with: (1) making certain that the generating/absorbing layer is long enough and strong enough to generate and dissipate waves, and (2) making sure that there is no significant re-reflection from free waves entering the sponge layer from the domain. Similar systems have been used with good results in compressible flow computational fluid dynamics to generate and absorb acoustic waves (Bodony, 2006), which are equivalent in many ways to shallow water equations.

Analytic proofs of the system are difficult nonlinearly, but systems are relatively straightforward to analyze for the case of a linear flat bed. However, although nonlinear analytics are difficult, demonstrations of nonlinear accuracy are not, as will be shown. Here, we perform analysis in one horizontal dimension for Boussinesq and shallow water systems although extension to two horizontal dimensions is straightforward. For a linear flat bed with one horizontal dimension, numerous sets of Boussinesq equations and shallow water equations may be represented as (e.g., following Wei and Kirby, 1999), after including the generating/absorbing terms,

$$\begin{aligned} \eta_{,t} + hU_{,x} + \alpha_1 h^3 U_{,xxx} &= \omega_1 (\eta_{imp} - \eta) \\ U_{,t} + g\eta_{,x} + \alpha h^2 U_{,xxt} &= \omega_1 (U_{imp} - U) + \omega_2 \alpha h^2 (U_{imp,xxt} - U_{,xxt}) \end{aligned} \quad (2.2)$$

where g is gravitational acceleration and h is the water depth. To obtain nonlinear shallow water equations, set $\alpha_1 = \alpha = 0$; for Nwogu's (1993) equations, $\alpha_1 = \alpha + 1/3$; to obtain Peregrine's (1967) depth-averaged equations, $\alpha_1 = 0$, $\alpha = -1/3$.

The undamped ($\omega_1 = \omega_2 = 0$) solution to these equations for free waves traveling in the positive and negative x-directions is

$$\begin{aligned} \eta_F &= \eta_0 \exp[i(kx - \sigma t)] + \eta_1 \exp[-i(kx - \sigma t)] + c.c. \\ U_F &= u_0 \exp[i(kx - \sigma t)] - u_1 \exp[-i(kx - \sigma t)] + c.c. \end{aligned} \quad (2.3)$$

where the radial frequency, σ , is given by

$$\sigma^2 = gk^2 \frac{1 - \alpha_1 (kh)^2}{1 - \alpha (kh)^2} \quad (2.4)$$

and k is the cross-shore wavenumber for a free wave. The relationship between velocities and surface elevations is

$$u_0 = \eta_0 \frac{gk}{\sigma(1 - \alpha(kh)^2)}. \quad (2.5)$$

Note again that these are also solutions to the damped equations if we take $\eta_{imp} = \eta_F$, and $U_{imp} = U_F$. Thus, the undamped result is a particular solution to the damped equation. To find the full solution to the damped equation, we merely need to find the homogeneous dissipative solution (with $\eta_{imp} = 0$, $U_{imp} = 0$) and apply boundary conditions based on the problem geometry. The homogeneous solution depends strongly on the spatial variation of the sponge layers,

$$\omega_1(x) = (\tilde{\omega}_1/L)f(x), \quad \omega_2(x) = (\tilde{\omega}_2/L)f(x) \quad (2.6)$$

where L is the length of the sponge layer.

Standard sponge layers typically are maximum at the computational boundaries, and have a smooth variation to zero at their furthest extent in the domain. Here, we assume a polynomial variation,

$$f(x) = (n+1) \left(\frac{x}{L}\right)^n, \quad 0 \leq x \leq L, \\ 0, \quad x < 0 \quad (2.7)$$

so that the integrated strength of the sponge layers $\int_0^L \omega_i dx = \tilde{\omega}_i$, $i = 1, 2$.

Analytical behavior of the generating-absorbing sponge layer is most easily demonstrated using the shallow water equations, as these have straightforward solutions. Details will differ once dispersive terms are added but, as will be shown, the behavior is generally similar although there are some significant differences; e.g., ω_2 has no effect on shallow water equations as there are no mixed space-time terms. In this case, the general solution to this system in the region $0 \leq x \leq L$ is, for η_{imp} and U_{imp} that satisfy the undamped equations,

$$\begin{aligned} \eta &= \tilde{\eta}_{impR} \exp(-ikx + i\sigma t) + \tilde{\eta}_{impL} \exp(ikx + i\sigma t) \\ &+ A_L \exp(ikx + i\sigma t) \exp\left(\frac{\tilde{\omega}_1}{L} C_0 \left(\frac{x}{L}\right)^{n+1}\right) \\ &+ A_R \exp(-ikx + i\sigma t) \exp\left(-\frac{\tilde{\omega}_1}{L} C_0 \left(\frac{x}{L}\right)^{n+1}\right) + c.c. \end{aligned} \quad (2.8)$$

$$\begin{aligned} U &= \tilde{\eta}_{impR} \sqrt{g/h} \exp(-ikx + i\sigma t) - \tilde{\eta}_{impL} \sqrt{g/h} \exp(ikx + i\sigma t) \\ &- A_L \sqrt{g/h} \exp(ikx + i\sigma t) \exp\left(\frac{\tilde{\omega}_1}{L} C_0 \left(\frac{x}{L}\right)^{n+1}\right) \\ &+ A_R \sqrt{g/h} \exp(-ikx + i\sigma t) \exp\left(-\frac{\tilde{\omega}_1}{L} C_0 \left(\frac{x}{L}\right)^{n+1}\right) + c.c. \end{aligned} \quad (2.9)$$

where $C_0 \equiv (gh_0)^{1/2}$ is the long wave speed.

This system has three parts: (1) undamped left-and-rightward moving imposed waves, (2) leftward-moving damped waves, and (3) rightward-moving damped waves. The general system plus boundary conditions will then give the performance of specific implementations. In the most simple, with $\eta_{imp} = U_{imp} = 0$, a rightward moving damped free wave that enters the sponge layer at $x = 0$ is reflected by a wall boundary at $x = L$, and re-exits moving leftward at $x = 0$ will be damped by a factor of $\exp[-2\tilde{\omega}_1/C_0]$. Thus, for a damping factor of $\tilde{\omega}_1/C_0 = 5$, the reflected wave will only be 4.5×10^{-5} times the size of the incoming wave, which is negligible.

To generate waves η_{impL} and U_{impL} (moving right to left in the negative x -direction), there are two likely boundary conditions:

1. $U = U_{impL}$ is imposed at the boundary, $x = L$, and U_{impL} and η_{impL} in the domain according to Eqs. (2.3–2.5).
2. U_{impL} and η_{impL} are imposed in the domain as before, with boundary conditions of $U = 0$ at $x = L$.

The first is trivial: from inspection $\eta = \eta_{impL}$ and $U = U_{impL}$ everywhere in the domain. If there are reflected waves entering the sponge layer, they will be damped, at least linearly, as before and will not interfere with the wave generation.

For the second boundary condition, imposing $U = 0$ on the boundary (wall) interferes with the desired $\eta = \eta_{impL}$ and $U = U_{impL}$ conditions, and the wall condition can only be satisfied by simultaneously generating a leftward-propagating decaying wave so that

$$\begin{aligned}\eta &= \tilde{\eta}_{impL} \exp(ikx + i\omega t) \left[\exp\left(\frac{\tilde{\omega}_1}{C_0} \left(\frac{x}{L}\right)^{n+1} - 1\right)\right] + c.c. \\ U &= -\tilde{\eta}_{impL} \sqrt{g/h} \exp(ikx + i\omega t) \left[\exp\left(\frac{\tilde{\omega}_1}{C_0} \left(\frac{x}{L}\right)^{n+1} - 1\right)\right] + c.c.\end{aligned}\quad (2.10)$$

The generated wave at $x = 0$ will have a relative error in height of $\exp[-\tilde{\omega}_1/C_0]$, which is exponentially double the error of the simple decaying wave entering from $x = 0$ and reflecting off the wall at $x = L$. For this reason boundary condition 1 is preferred if possible, although the wall condition will also work well as will be shown.

These examples have been for linear shallow water equations, where closed-form analytical solutions are readily available, but analyses will be performed numerically in the next section for dispersive Boussinesq systems. The most important difference here is that Boussinesq systems will experience reflections from the boundary between damped and undamped zones, while shallow water equations cannot, at least for one horizontal dimension. Because of this, constant-strength sponge layers should not be used for dispersive Boussinesq systems: however, with linear and quadratic polynomial sponge layers can both work well. If the absorbing-generating sponge layer is long enough and strong enough, the details cease to matter and waves will be absorbed and generated accurately.

Of course, for any system it is necessary to know the dispersion relation and the relationship between surface elevations and velocities to force $\tilde{\eta}_{imp}$ and U_{imp} , but these relations may readily be determined for most cases. Irregular waves may also be easily generated by the superposition of various frequencies using standard methods. The damping nature of the sponge layer further appears to almost eliminate the high frequency noise generated by some methods, which is a welcome side effect.

The second major advantage of this type of generation system is that it is relatively straightforward to generate nonlinear waves at the same time as reflected waves are absorbed. If a nonlinear solution is known for an undamped Boussinesq or other system, it may simply taken to be the imposed solution and there are no further changes. The nonlinear waves will then be generated in the same way as linear waves. This may be done for both regular waves, and for unsteady nonlinear waves if the appropriate undamped solutions are known. It should be emphasized that the nonlinear solutions must be for the specific system modeled and using, for example, second order hyperbolic Stokes solutions for a Boussinesq model will give worse results than a second order solution of that Boussinesq system.

2.1. Relationship to relaxation zones

Although it may not be immediately obvious, the generating-absorbing sponge layers presented here have links to relaxation zones (Madsen et al., 2003). In these zones, systems are computed as normal,

but the computed solution is replaced with a blend of the undamped and imposed solutions at the end of each time step. This may be written as

$$\mathbf{a}(x, y, t + \Delta t) \equiv c_r(x, y) \mathbf{a}_u(x, y, t + \Delta t) + (1 - c_r(x, y)) \mathbf{a}_{imp}(x, y, t + \Delta t) \quad (2.11)$$

where $\mathbf{a}_u(x, y, t + \Delta t)$ is the quantity that would arise at the end of each time step from the undamped, unforced equations, $\mathbf{a}_{imp}(x, y, t)$ is the vector of imposed quantities, and $0 \leq c_r(x, y) \leq 1$ is the spatially-varying relaxation coefficient, with $c_r = 0$ forcing the solution exactly to the target, and $c_r = 1$ leaving the solution unchanged. Using this method, solutions are gradually forced to the desired quantities.

If we expand all quantities with Taylor series in time, so that $\mathbf{a}(t + \Delta t) = \mathbf{a}(t) + \mathbf{a}_t(t)\Delta t + O(\Delta t^2)$ and similarly for the undamped and imposed systems $\mathbf{a}_u(x, y, t)$ and $\mathbf{a}_{imp}(x, y, t)$, the relaxation zone equations may be written as (remembering that $\mathbf{a}(t) = \mathbf{a}_u(t)$ at the beginning of each time step)

$$\mathbf{a}_{,t} = c_r \mathbf{a}_{u,t} + (1 - c_r) \mathbf{a}_{imp,t} + (1 - c_r) \frac{(\mathbf{a}_{imp} - \mathbf{a})}{\Delta t} \quad (2.12)$$

and compared to the present generating-absorbing sponge layers which, in the same format, may be written as, if $\omega_2 = 0$,

$$\mathbf{a}_{,t} = \mathbf{a}_{u,t} + \omega_1 (\mathbf{a}_{imp} - \mathbf{a}). \quad (2.13)$$

Thus, there are two differences between the two systems. The first is that performance in the relaxation zone has a dependence on time step, Δt , which makes the system more damped/forced for short time steps, and less damped for large time steps. In contrast, the present system is invariant with respect to time step. The second difference is that the relaxation zone directly imposes a component of $\mathbf{a}_{imp,t}$ while the present system does not. Of the two, the relaxation zone dependence on time step is the most significant and the system presented here will have more predictable properties. However, a choice of relaxation coefficient, c_r that varies with time step can make the system equivalent to the present ω_1 damping: if we define $1 - c_r = \omega_1 \Delta t$, then Eq. (2.12) becomes

$$\mathbf{a}_{,t} = (1 - \omega_1 \Delta t) \mathbf{a}_{u,t} + (\omega_1 \Delta t) \mathbf{a}_{imp,t} + \omega_1 (\mathbf{a}_{imp} - \mathbf{a}) \quad (2.14)$$

which is in the limit of small Δt equivalent to the present ω_1 damping (Eq. (2.13)).

3. Frequency-domain linear wave generation and damping coefficients for Boussinesq-type equations

Although reflection and generation coefficients may be found analytically for the linear shallow water equations, general analytical solutions do not appear simple for the wide variety of systems that may be encountered. Here, we present numerical frequency-domain generation and damping coefficients for the Boussinesq-type systems of Eq. (2.2). These have higher derivatives than shallow water equations, which produce somewhat different performance although general trends are similar. Linear reflection coefficients were generated using standard methods by assuming periodic waves over a flat bed, and then solving the resulting coupled ordinary differential equations using centered finite differences with a wall boundary condition at the end of the sponge layer, $x = L$, and by assuming free waves satisfying Eqs. (2.3–2.5) at the interior boundary, which was five water depths past the sponge layer. Imposed waves were homogeneous solutions to the appropriate sets of equations, and all numerical solutions were tested for convergence.

Sponge layers were assumed to have forms according to Eqs. (2.6–2.7) with varying lengths, L , polynomial coefficients, n , and integrated strengths, $\tilde{\omega}_1$ and $\tilde{\omega}_2$. The analysis of Section 2 with the shallow water equations suggests that wave generation is more of a challenge for a wall boundary condition, so this will be the focus of our analysis.

3.1. Generation coefficients

Fig. 1 shows wave generation coefficients for Nwogu's equations with Padé [2, 2] dispersion, with sponge lengths of $L = (2.5, 5, 10, 20)h$, and integrated sponge strengths of $\tilde{\omega}_1/(gh)^{1/2} = (2.5, 5, 10)$. For this first test we set $\tilde{\omega}_2/(gh)^{1/2} = 0$, and the polynomial in Eq. (2.7) has the quadratic variation $n = 2$. Several separate progressions towards more accurate generation may be seen. First, as integrated sponge strength increases from $\tilde{\omega}_1/(gh)^{1/2} = 2.5$ to 10, the generation coefficient becomes much closer to 1 as expected from the analytical shallow water equation solutions. A strength of $\tilde{\omega}_1/(gh)^{1/2} = 10$ appears to give accurate generation for all but the shortest sponge length, $L = 2.5h$ and even here the maximum error is less than 1% over the range $kh = [0, 4]$. Generation accuracy increases with increasing sponge length up to $L = 10h$, but is essentially constant for longer sponges. One unexpected but highly welcome observation is that, except for the shortest sponge layer of $L = 2.5h$, dispersive waves are generated more accurately than shallow water waves. This means that the shallow water generation results of the previous section may be used conservatively to guide wave generation in other systems. Note also that the low wave-number Boussinesq results match well the shallow water solutions for $L = 20h$ and $L = 10h$, but less well for other sponge layer lengths. This is because both the wavelength and sponge layer length scales are important: both need to be near the shallow water range to be suitable predictors for Boussinesq results.

The results of Fig. 1 are quite good, but used a damping coefficient $\tilde{\omega}_1$ that only affects pure time derivative terms. Including mixed space–

time derivative damping, $\tilde{\omega}_2$, may add significant complexity to coding but could potentially also increase generation accuracy enough to make it worthwhile. Fig. 2 shows generation coefficients using $\tilde{\omega}_1 = \tilde{\omega}_2$ for otherwise the same conditions as in Fig. 1. Unfortunately, the hoped-for increase in accuracy does not materialize. Results for low wavenumber and short sponge lengths in particular are considerably worse than the $\tilde{\omega}_2 = 0$ case, and it does not appear that $\tilde{\omega}_2$ offers advantages for wave generation.

Comparison of linear and quadratic ($n = 1, 2$) sponge layer polynomials in Fig. 3 shows little difference in performance between the two sponge layer shapes except for very short sponge layers that would not be recommended in any case. Thus, the detailed shape of the sponge layer has little influence on linear wave generation properties. However, we do note without showing results that a constant sponge layer ($n = 0$) should not be used.

Fig. 4 compares generation coefficients for Peregrine's and Nwogu's equations. Again, details differ but trends are identical, and both sets of equations give excellent results for strong and long sponge layers. One interesting detail is that Peregrine's equations appear to generate short waves more accurately than Nwogu's equations, for reasons that are unclear.

3.2. Reflection coefficients

Fig. 5 shows reflection coefficients for Nwogu's equations for sponge layers of different lengths and strengths, both using $\tilde{\omega}_2 = 0$ and $\tilde{\omega}_2 = \tilde{\omega}_1$. These results are surprising in many ways. For $\tilde{\omega}_2 = 0$, all sponge layer strengths $\tilde{\omega}_1$ show major differences from the analytical shallow water equation values, particularly for short sponge layers with $L \leq 5h$. Here, strong sponge layers have more reflection than weaker sponge layers, and all sponge strengths show significant reflection. This general result has been known to practicing modelers, who have learned to not use short sponge layer lengths, but has never previously been quantified. In

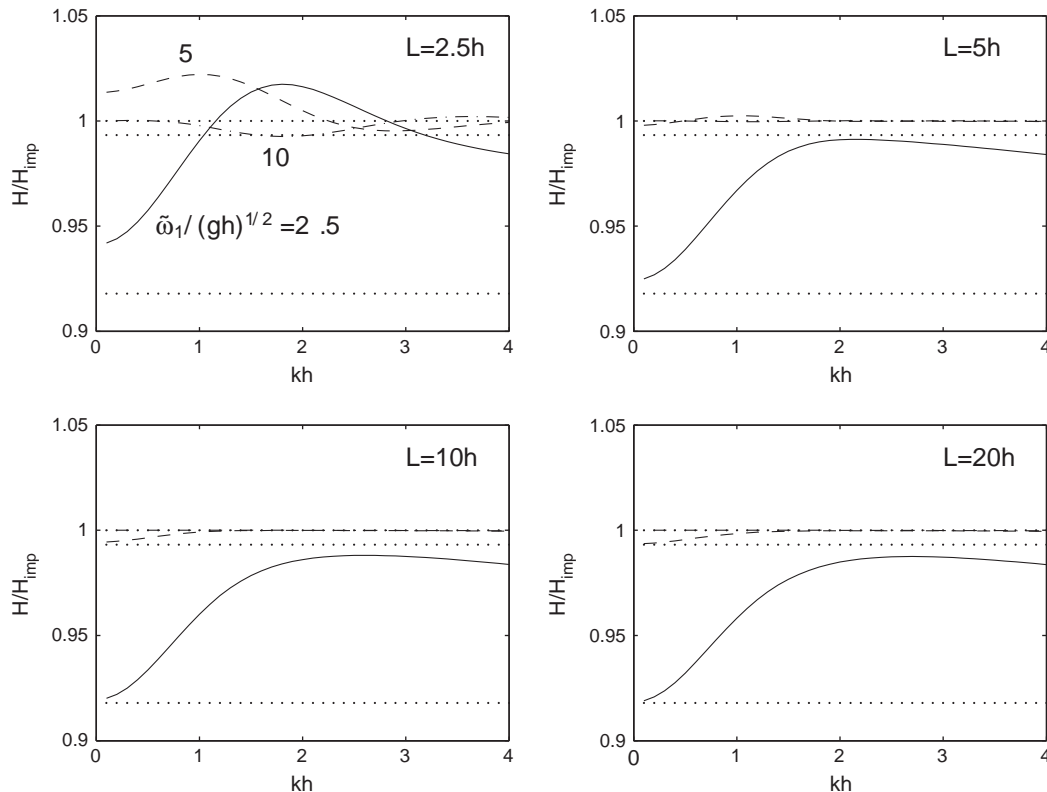


Fig. 1. Wave generation coefficients for $\tilde{\omega}_1/(gh)^{1/2} = 2.5(-), 5(- -), 10(- \cdot -)$, using Nwogu's equations, $n = 2, \tilde{\omega}_2 = 0$. Shallow water equation results are shown as dotted lines.

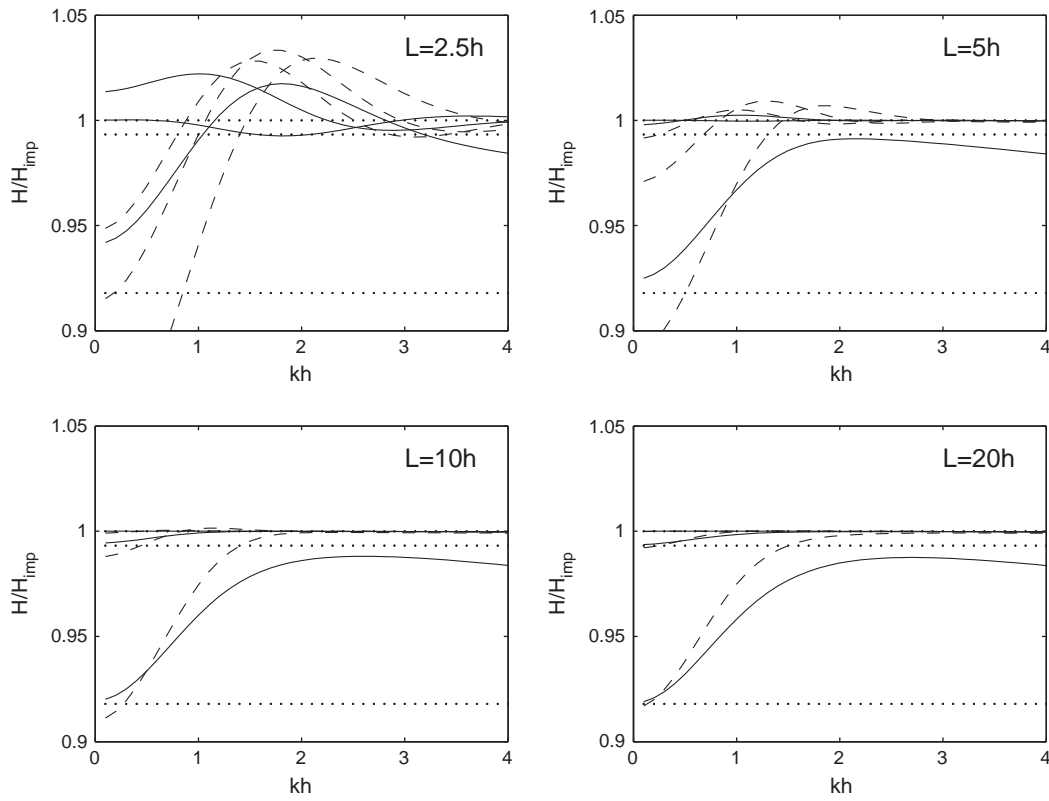


Fig. 2. Comparison of wave generation coefficients for $\tilde{\omega}_2/(gh)^{1/2} = \tilde{\omega}_1/(gh)^{1/2}$ (---); $\tilde{\omega}_2/(gh)^{1/2} = 0$ (—). Other parameters are identical to Fig. 1.

contrast, including $\tilde{\omega}_2 = \tilde{\omega}_1$ in computations tends to decrease significantly the reflection coefficients, particularly for strong sponge layers. With sponge lengths of $L = 10h$ and $\tilde{\omega}_2 = 0$, reflection coefficients of

$R \leq 0.01$ are possible for all wavenumbers using just $\tilde{\omega}_1$; however including $\tilde{\omega}_2 = \tilde{\omega}_1$ allows reflection coefficients more than 10 times smaller for the same conditions.

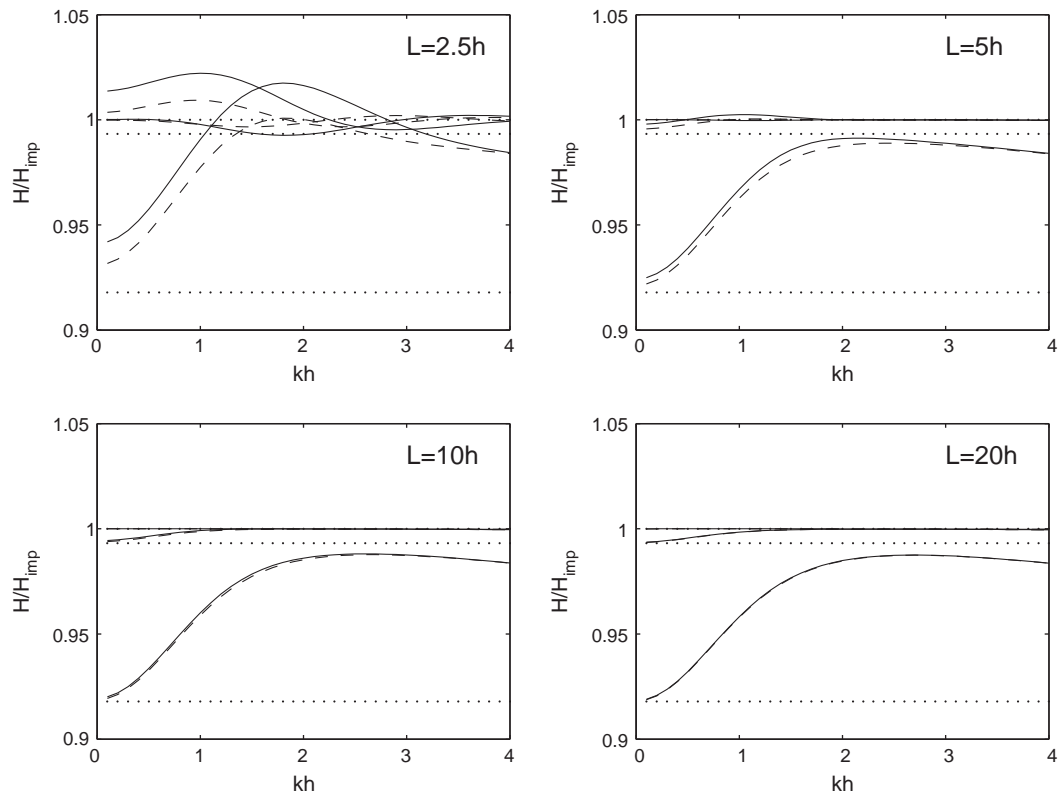


Fig. 3. Comparison of wave generation coefficients for polynomial coefficients $n = 1$ (---), $n = 2$ (—). Other parameters are identical to Fig. 1.

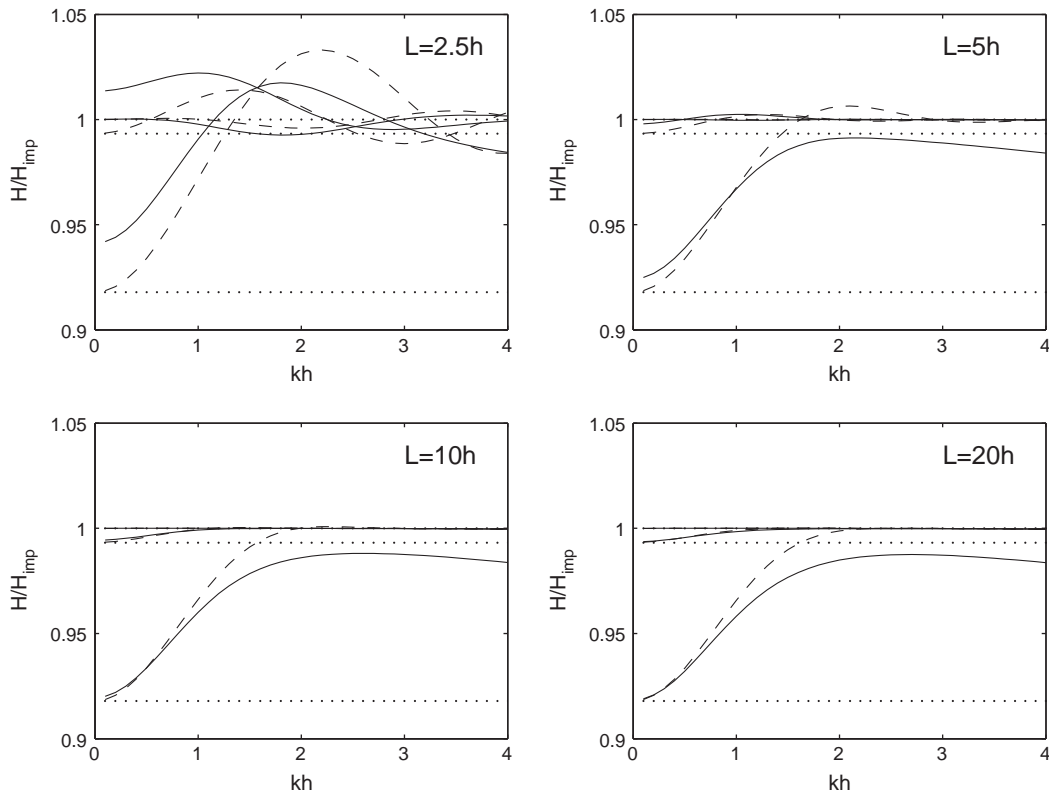


Fig. 4. Comparison of wave generation coefficients for Peregrine's equations (—), Nwogu's equations (---). Other parameters are identical to Fig. 1.

Taken together, results show that waves may be generated and absorbed accurately for different systems if two conditions are satisfied: (1) the sponge layer is long enough; and (2) the integrated strength of

the sponge layer is large enough. Equation details and sponge layer profiles are very much secondary once these criteria have been satisfied. Good results will be given for a variety of systems by a length $L = 10h$,

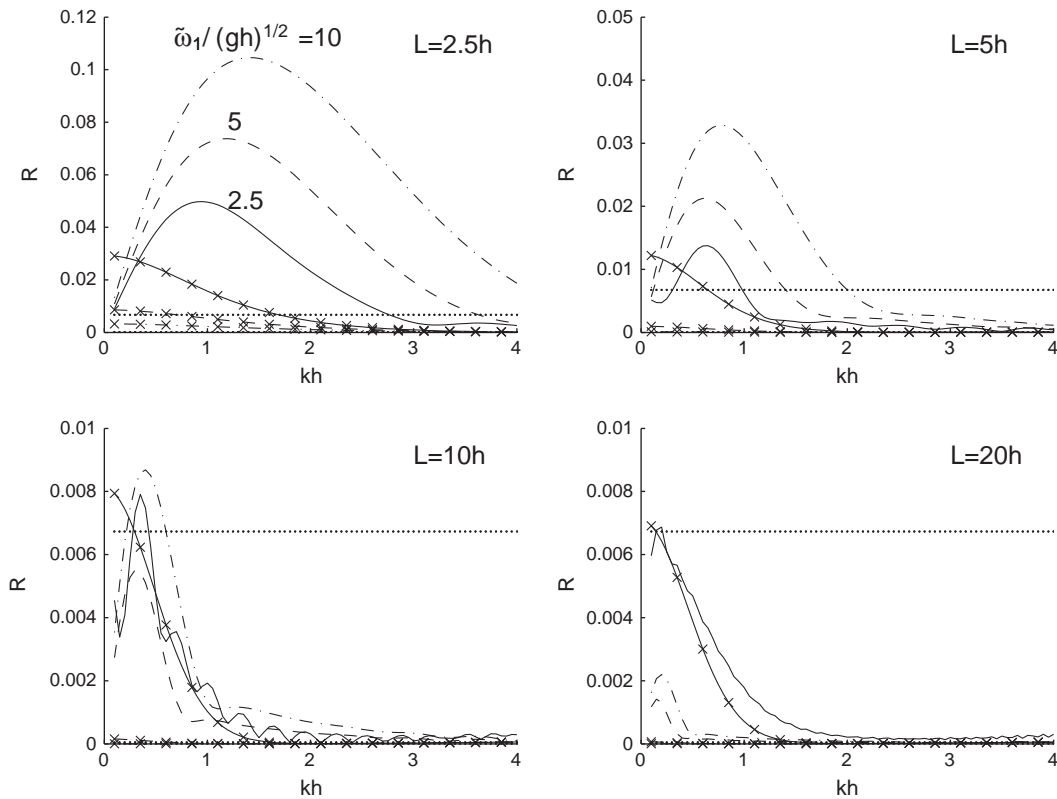


Fig. 5. Reflection coefficients for $\tilde{\omega}_1/(gh)^{1/2} = 2.5$ (—), 5 (---), 10 (---), using Nwogu's equations, $n = 2$. (no symbol) $\tilde{\omega}_2 = 0$; (x) $\tilde{\omega}_2 = \tilde{\omega}_1$. Shallow water equation results are shown as dotted lines.

and $\tilde{\omega}_1/(gh)^{1/2} = 5$, which will give less than 1% error in both reflection and generation. Higher order derivative terms included in $\tilde{\omega}_2$ may be neglected without negative effects for wave generation, but these terms will act to reduce reflections significantly when they are included.

4. Time domain numerical simulations

Frequency domain solutions for wave generation showed good properties, but still require validation in the time domain numerical models used for computing nonlinear, phase-resolving wave transformation. One important result from the previous section was that generation coefficients based on shallow water equation results appear conservative for all dispersive models tested if the layer is at least $L = 5h$ long. In contrast, longer lengths of at least $L = 10h$ are required to give low reflection if only ω_1 is used, but adding $\omega_1 = \omega_2$ decreases reflections considerably.

With this in mind, and to demonstrate that the concept may be applied to almost any system, we apply generating–absorbing sponge layers to the $O(\mu^2)$ rotational Green–Naghdi–Boussinesq model of Zhang et al. (2013). The Green–Naghdi–Boussinesq systems of Zhang et al. (2013) are related to the Boussinesq systems of Nwogu (1993) and Wei et al. (1995), but with no assumption of irrotationality. They retain the ability to manipulate properties through asymptotic rearrangements for dispersion and shoaling and obtain Padé approximants for appropriate dispersion levels. The inviscid $O(\mu^2)$ equations (no eddy viscosity or bottom stress), and including ω_1 but not ω_2 terms, may be written in the general form of

$$\eta_{,t} + \nabla \cdot \left(\sum_{n=0}^N \mu^{\beta_n} \mathbf{u}_n(\eta + h) \mathbf{g}_n |_{q=1} \right) = \omega_1 (\eta_{imp} - \eta) \quad (4.1)$$

$$\begin{aligned} &(\eta + h) \sum_{n=0}^N \phi_{mn} u_{n,t} + \text{other terms} \\ &= (\eta + h) \sum_{n=0}^N \omega_1 (u_{n-imp} - u_n) \phi_{mn}, \quad m = 0, 1, 2, \dots, N \end{aligned} \quad (4.2)$$

where $N = 2$ for $O(\mu^2)$ equations, and full details and coefficients are given in Zhang et al. (2013).

The computational domain shown in Fig. 6 consists of 3 parts: wavemaker region ($L_1 = 5$ m), propagating part ($L_2 = 32$ m) and absorbing sponge layer ($L_3 = 10$ m). Both linearly-varying and

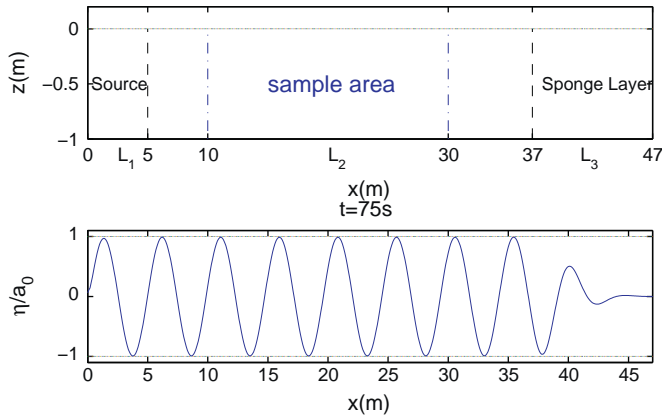


Fig. 6. The domain computational and linear wave generation.

quadratically-varying ω_1 were used as defined in Eqs. (2.6–2.7), as given by

$$\begin{aligned} \eta_{imp}, u_{n-imp} &= \begin{cases} \eta_{imp}, u_{n-imp} & 0 \leq x \leq L_1 \\ 0 & x > L_1 \end{cases}; \\ \omega_1(x) &= \begin{cases} \frac{\tilde{\omega}_1}{L_1} (n+1) \left(1 - \frac{x}{L_1}\right)^n & 0 \leq x \leq L_1 \\ 0 & L_1 < x < L_2 \\ \frac{\tilde{\omega}_1}{L_3} (n+1) \left(\frac{x-L_1-L_2}{L_3}\right)^n & x \geq L_3 \end{cases} \end{aligned} \quad (4.3)$$

where $\tilde{\omega}_1/(gh)^{1/2} = 10$ for all cases. For both generation and absorption sponge layers, $\tilde{\omega}_2/(gh)^{1/2} = 0$. Wall boundary conditions were used for all tests. Fig. 6 shows a first test of generation using a very small monochromatic wave, with $H = 0.0001$ m, $h = 1$ m, and $T = 1.91$ s ($kh = 1.29$), demonstrating generation, propagation, and absorption.

4.1. Accuracy of regular wave generation

The accuracy of regular wave generation is the most basic test of the new system. Imposed quantities were obtained from Stokes-type expansions of the equations of Zhang et al. (2013), where either the linear or second order imposed solutions were used over a range of wave heights. Coefficients and forms for these velocities and surface elevations follow Zhang et al. (2013), which may be consulted for more details. Note again that surface elevations and velocities are *not* the same as found by a standard Stokes expansion (e.g., Dean and Dalrymple, 1991) – imposed surface elevations and velocities must be solutions to the approximate Boussinesq system, which differ somewhat from the arbitrary depth hyperbolic solutions.

Wave heights were recorded as the crest to trough elevation (averaged over 5 wave periods) at each point along the 20 m sample area shown in Fig. 6. These heights varied in space because of unwanted reflections, and nonlinearly-generated spurious harmonics. Fig. 7 shows maximum and minimum wave heights measured over this sample region for waves with varying height/depth ratios. The maximum and minimum of these wave heights over the sample area and their differences from target values provide quantitative measures of the combined generation–reflection error. In addition to the spatially-varying

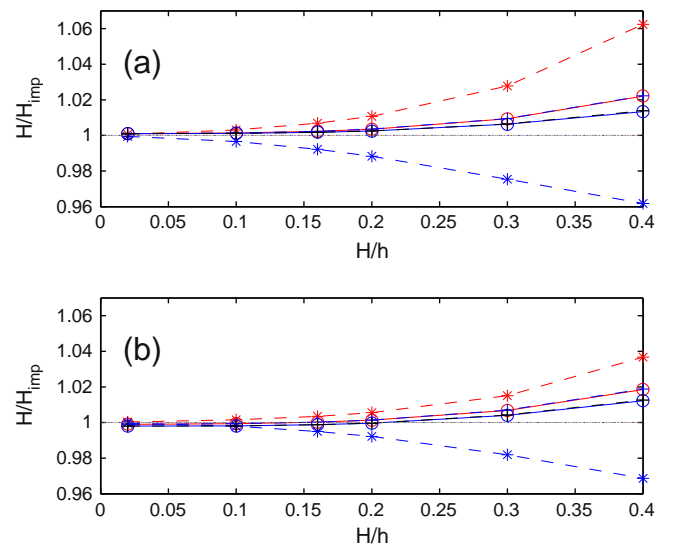


Fig. 7. Maximum and minimum wave heights recorded over the 20 m sample area of Fig. 6 using linear and second order generation and absorption. (a) Linearly varying sponge layers; (b) quadratically varying sponge layers. (–*–) Maximum and minimum heights for first order generation; (–o–) second order generation; and (–+–) second order generation using relaxation zones (obscured).

error, there could also be linear and nonlinear errors in average wave height.

The situation is simplest for the smallest wave heights where linear considerations dominate. Here, combined generation and reflection errors are of $O(0.1\%)$ using linear and nonlinear imposed values, and for linear and quadratic sponge layer spatial variations. These results correspond well to frequency domain solutions shown in Figs. 3 and 5, which predict very accurate generation for $kh = 1.29$ using $\tilde{\omega}_1/(gh)^{1/2} = 10$, and $L = 5h$, and minimal reflections using $\tilde{\omega}_1/(gh)^{1/2} = 10$, and $L = 10h$. This good correspondence in accuracy occurs even though frequency domain results used Nwogu's equations while the time domain results use the equations of Zhang et al. (2013). When combined with Fig. 4 showing the similar accuracy of generation for Peregrine's equations, results suggest that the broad zones of high and low accuracy generation and reflection have only a weak dependence on the particular Boussinesq-type equations used, and that Figs. 1–4 may be used as a guide for many types of Boussinesq equations.

Errors increase with increasing wave height for both linear and quadratic sponge layers, and for linear and second order imposed waves. This implies that the larger wave height errors arise from errors in the generation of nonlinear harmonics. For the linearly-varying sponge layers ($n = 1$), Fig. 7(a) shows envelope errors at $H_{imp}/h = 0.4$ spanning $[-4, +6]\%$ using first order generation, and $[+1, +2]\%$ using second order generation. Thus, the second order generation shows a large improvement in accuracy, with remaining errors arising from neglected third and higher harmonics: stream function wave theory (Fenton, 1988) gives a third harmonic for $H/h = 0.4$ and $kh = 1.29$ with magnitude 6.5% of the first harmonic, so neglect of third and higher harmonics is substantial here. Further increases in accuracy for nonlinear generation are almost certain if more harmonics are included. Using the quadratically-varying sponge layers ($n = 2$) in Fig. 7(b) gives lower errors for both the linear and second order imposed wave properties, but differences are relatively small.

Fig. 8 shows surface elevation time series comparisons at $x = 10$ m between linear generation, nonlinear generation, and the target second order solution for a significantly nonlinear wave with $H/h = 0.4$. The nonlinear solution clearly shows a much better profile, with the expected sharper crest and flatter trough. While linear generation does a reasonable job with the overall wave height at this location, its profile is not good and the spuriously generated free harmonics will cause wave heights to vary over space. This is exactly the situation where the new generation method works well, and demonstrates its utility.

Finally, Fig. 7 gives a comparison between sponge layers using second order generation with linearly varying sponge layers, and the Madsen relaxation method using $1 - c_r = \omega_1 \Delta t$ as suggested in Section 1 and with the same imposed waves. Results are close to identical, demonstrating the correspondence between the two methods once coefficients are adjusted

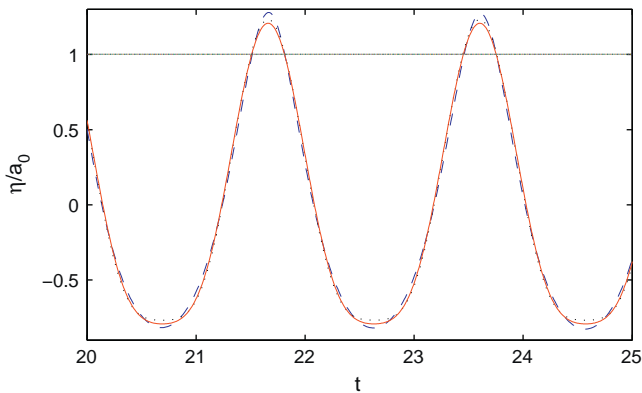


Fig. 8. Elevation time series at $x = 10$ m with $H/h = 0.4$, $kh = 1.29$ and linear sponge layer. (—) Second order target wave; (---) generated wave using linear imposed signal; and (· · ·) generated wave using second order nonlinear imposed signal.

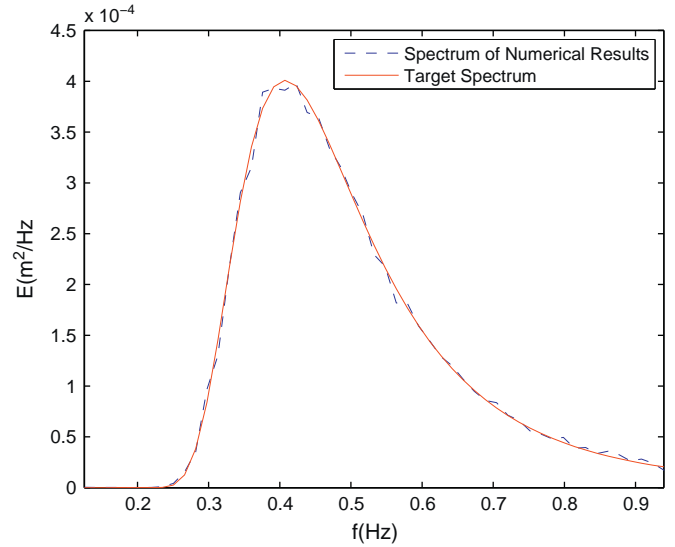


Fig. 9. Target (—) and generated (---) energy density spectra at $x = 10$ m.

appropriately. The only significant difference is that the original relaxation method will have a dependence on time step if used with a constant c_r , while the sponge layers presented here have properties that are independent of time step.

4.2. Random wave generation

All waves in nature are random, and the present method can simulate random waves when given properly imposed elevations and velocities. For small amplitude waves, these are simply linear superpositions of regular waves and will have similar properties,

$$\eta_{imp} = \sum_i \eta_i \cos(k_i x - \sigma_i t + \epsilon_i) \quad (4.4)$$

$$u_{n-imp} = \sum_i \sum_{n=1}^N u_{n,i} \cos(k_i x - \sigma_i t + \epsilon_i) \quad (4.5)$$

where the continuous spectrum is here discretized into a large number of frequencies with specified amplitude and random phase shift for numerical purposes.

Random wave capability was tested using a JONSWAP target spectrum for very small waves with heights $H_{RMS}/h \approx 0.01$, peak period $T_p = 2.5$ s, and over the same topography as in Fig. 6. These are small enough that nonlinear terms are negligible and the test is effectively linear. Fig. 9 shows the comparison between computed and target spectra: computed results agree almost exactly with the target over a wide range of frequencies. Time series comparisons in Fig. 10 also show excellent correspondence. This gives good confidence moving forward for application in other areas.

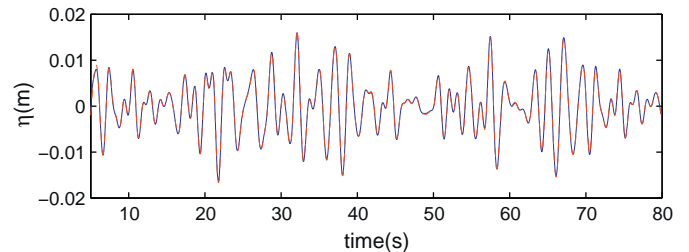


Fig. 10. Computed (—) and target (---) time series of small irregular waves at $x = 10$ m.

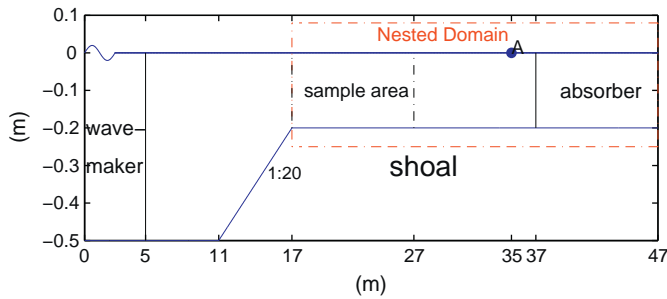


Fig. 11. Irregular nonlinear wave generation test set-up.

The generation test with small amplitude waves is useful, but it may be desired in some instances to generate significantly nonlinear irregular waves. The generating–absorbing sponge layer can do this provided that accurate target time series are known, which is not at all simple. A full second order Stokes analysis of a system including super-and-subharmonics can provide this in many circumstances, but these analyses are known to break down in shallow water where they are most needed, and general characteristics of fully nonlinear irregular wave target time series are still not known a priori for most instances. However, there are still circumstances where this might be accomplished.

Here, we demonstrate an application of the absorbing–generating sponge layer for taking nonlinear irregular waves generated in one domain, and reproducing them in another as might be done using nested grids. Fig. 11 shows the computational setup. In the large domain, $0 \text{ m} \leq x \leq 47 \text{ m}$, irregular waves are generated over the range $0 \text{ m} \leq x \leq 5 \text{ m}$, and subsequently propagate up to a shoal that is $2/5$ of the original depth, where waves become highly nonlinear. A nested domain on top of the shoal, $17 \text{ m} \leq x \leq 47 \text{ m}$, is then simulated by using recorded values for the large domain between $17 \text{ m} \leq x \leq 27 \text{ m}$ as imposed values for the nested domain. The accuracy of this nonlinear, irregular wave generation is shown in Fig. 12 by comparing first generation (large domain) and second generation (nested domain) values at $x = 35 \text{ m}$. The two generations are virtually identical, demonstrating that the absorbing–generating sponge layer can accurately reproduce highly nonlinear irregular waves when given a proper signal. However, as noted earlier, the specification of a proper nonlinear wave signal remains an open question in many cases.

5. Conclusions

The generating–absorbing sponge layers developed here give good results for several phase-resolving wave systems tested and would likely work well for numerous other systems. They are relatively straightforward to implement, requiring only a knowledge of free waves which are well known for many systems, and can accurately reproduce nonlinear free waves if given appropriate signals at least up to $H/h = 0.4$.

Wave generation can be accomplished well using just the ω_1 source zones (operating on pure time derivative terms), but damping appears to be more efficient when using both ω_1 and ω_2 (mixed space–time)

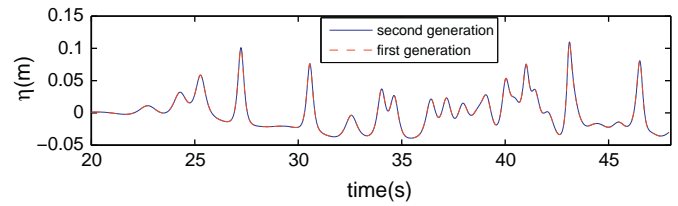


Fig. 12. Irregular nonlinear wave time series at location A.

terms. Wave generation for dispersive systems appears to be in general more efficient than is predicted by shallow water equations, while reflection coefficients for dispersive systems tend to be much higher than predicted by shallow water equations. Good results may be found for all systems tested using lengths of $L = 10h$, and integrated strengths of $\tilde{\omega}_1/(gh)^{1/2} = 5-10$. With appropriate choice of coefficients, the sponge layer systems shown here have a strong correspondence to relaxation zones for wave generation, and similar performance.

All analyses and simulations here have been performed for one horizontal dimension, but techniques and conclusions should carry over to two dimensions with minimal modification.

Acknowledgments

This work was funded under the National Science Foundation grant 1025519, and by the Office of Naval Research under the awards N00014-11-1-0045 and N00014-13-1-0123. Their support is gratefully acknowledged.

References

- Bodony, D.J., 2006. Analysis of sponge zones for computational fluid mechanics. *J. Comp. Phys.* 212, 681–702.
- Chawla, A., Kirby, J.T., 2000. A source function method for generation of waves on currents in Boussinesq models. *Appl. Ocean Res.* 22, 75–83.
- Dean, R.G., Dalrymple, R.A., 1991. *Water Wave Mechanics for Engineers and Scientists*. World Scientific Publishing Co., Singapore.
- Fenton, J.D., 1988. The numerical-solution of steady water-wave problems. *Comput. Geosci.* 14, 357–368.
- Kennedy, A.B., Fenton, J.D., 1997. A fully nonlinear numerical method for wave propagation over topography. *Coastal Eng.* 32, 137–161.
- Larsen, J., Dancy, H., 1983. Open boundaries in short-wave simulations – a new approach. *Coastal Eng.* 7, 285–297.
- Israeli, M., Orszag, S.A., 1981. Approximation of radiation boundary conditions. *J. Comp. Phys.* 41, 115–135.
- Madsen, P.A., Bingham, H.B., Schaffer, H.A., 2003. Boussinesq-type formulations for fully nonlinear and extremely dispersive water waves: derivation and analysis. *Proc. R. Soc. A.* 459, 1075–1104.
- Nwogu, O., 1993. Alternative form of Boussinesq equations for nearshore wave propagation. *J. Waterw. Port Coast. Ocean Eng.* 119, 618–638.
- Peregrine, D.H., 1967. Long waves on a beach. *J. Fluid Mech.* 27, 815–827.
- Skotner, C., Apelt, C.J., 1999. Internal wave generation in an improved two-dimensional Boussinesq model. *Ocean Eng.* 26, 287–323.
- Wei, G., Kirby, J.T., Grilli, S.T., Subramanya, R., 1995. A fully nonlinear Boussinesq model for surface-waves. 1. Highly nonlinear unsteady waves. *J. Fluid Mech.* 294, 71–92.
- Wei, G., Kirby, J.T., 1999. Generation of waves in Boussinesq models using a source function method. *Coast. Eng.* 36, 271–299.
- Zhang, Y., Kennedy, A.B., Panda, N., Dawson, C., Westerink, J.J., 2013. Boussinesq–Green–Naghdi rotational water wave theory. *Coast. Eng.* 73, 13–27.